IEICE Communications Express, Vol.12, No.12, 633–636

ComEX

LETTER

Suppression of azimuth ambiguity for the detection of ships on the ocean by wide-swath synthetic aperture radar

Tomoya Yamaoka[1, a)] **and Satoshi Kageme**[2]

Abstract This study proposes the suppression of the azimuth ambiguity with high azimuth resolution and signal-to-noise ratio in an image captured at a low pulse repetition frequency for the detection of ships on the ocean with wide swath by spaceborne synthetic aperture radar (SAR). The proposed scheme can reduce the azimuth ambiguity by processing the two images divided in the Doppler frequency region, which selects pixels with smaller values between the two images and derives their gains. After evaluating the proposed scheme, we discovered that azimuth ambiguity can be suppressed, and the expected swath of the observed image is equivalent to five times that of the conventional SAR image. The proposed scheme improved the signal-to-azimuth ambiguity power ratio by 27.7 dB.

Keywords: azimuth ambiguity, ship detection, synthetic aperture radar (SAR), wide-swath

Classification: Sensing

1. Introduction

Synthetic aperture radar (SAR) is crucial in remote sensing because the target can be observed through images, regardless of daylight conditions [1]. This study focuses on detection ships on the ocean using spaceborne SAR. A low pulse repetition frequency (PRF) must be set to lengthen the pulse repetition interval (PRI) to realize wide-area observations by SAR. However, if PRF is set to a low value, the number of sampling points in the azimuthal direction decreases. Therefore, the Doppler frequency component obtained through the fast Fourier transform (FFT) resulting in aliasing, and unnecessary signal components, called azimuth ambiguities, are generated in the SAR image, degrading the image visibility. scanSAR [2] can widen the observation area without generating azimuth ambiguity but degrades azimuth resolution and signal power. This study investigates the suppression of the azimuth ambiguity for SAR images with higher azimuth resolution and S/N ratio by inserting 0s into the slow time direction of the signals at a low PRF.

In conventional studies of azimuth ambiguity, various types of systems such as the moving target indicator [3], polarization SAR [4], and bistatic SAR [5] have also been investigated. Azimuth ambiguity reduction using a winner filter is a typical method [6, 7, 8]. However, these methods are not aimed at widening the observation areas with low PRF.

Multichannel SAR technology [9] can be used to reduce azimuth ambiguity for a wide-swath SAR. However, the suppression of azimuth ambiguity to widen the observation area requires multiple receivers and high sampling in the azimuthal direction. Some azimuth ambiguity reduction schemes use compressed sensing [10, 11] to widen the observation area with a single receiver. However, compressive sensing requires repetition of the imaging and inverse imaging processes 30 times, which increases the number of calculations required and the processing delay. Currently, the number of swaths can only be doubled.

Thus, we propose a scheme to process the images obtained by dividing the Doppler frequency component into two components to suppress the azimuth ambiguity generated by low-PRF wide-ocean observations at a low cost. The scheme focuses on the phenomenon in the range-Doppler frequency region of an SAR image with a low PRF. In the image obtained by dividing the Doppler frequency component into two components, sufficient power is provided to both pixels at the pixel position where the target exists. Conversely, the pixel in which azimuth ambiguity exists has less power on one side. As a result, we propose a scheme to suppress the azimuth ambiguity in SAR images. The azimuth ambiguity of ships and land can be suppressed, and ships in wide-area oceans at a low PRF can be detected using the proposed scheme. In the demonstration using the SAR image of TerraSAR-X, azimuth ambiguity was suppressed with a swath five times. The remainder of this paper is organized as follows. The proposed scheme is explained in Section II and demonstrated in Section III. Finally, Section IV concludes the study.

2. Proposed scheme

This section describes the proposed scheme, its preconditions, problem awareness, concept, and specific processing flow.

2.1 Precondition

In this study, the signals observed through the strip map with less azimuth ambiguity were thinned to $1/M$ (M is a natural number) in the slow time direction. Therefore, PRI is set to M times, and PRF is set to $1/M$ times. Suppose f_p is the reduced PRF value. Aliases occur in the signals owing to the low PRF and the swath width will be M times larger than

[1] Information Technology Research and Development Center, Mitsubishi Electric Corporation, Kamakura 247–8501, Japan
[2] Kamakura Works, Mitsubishi Electric Corporation, Kamakura 247–8520, Japan
[a)] Yamaoka.Tomoya@ab.mitsubishielectric.co.jp

DOI: 10.23919/comex.2023XBL0109
Received August 18, 2023
Accepted September 6, 2023
Publicized October 17, 2023
Copyedited December 1, 2023

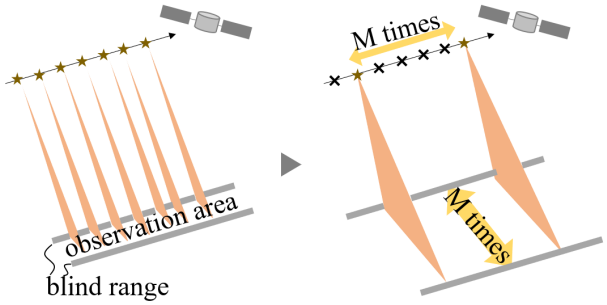

Fig. 1 Explanation of wide swath. The satellite has a longer PRI and a larger observation area.

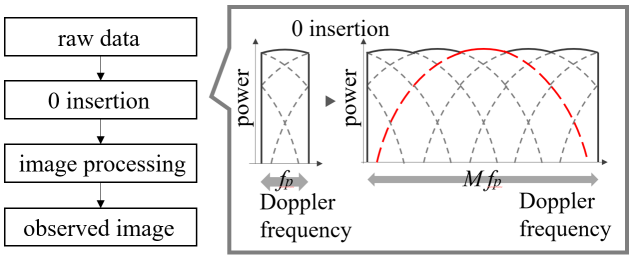

Fig. 2 Precondition. The insertion of 0s discretizes the signal in the slow time direction. Replicas of the signal occur on the Doppler frequency, improving azimuth resolution, and signal power.

the normal observation width, as shown in Fig. 1.

The preconditions are shown in Fig. 2. Image processing was performed after inserting (M-1) 0s between the signals in the slow time direction. The insertion of 0s discretized the signal in the slow time direction. Therefore, the PRF in the Doppler frequency is increased by inserting 0s, and replicas of the signals occur at the Doppler frequency, as shown in Fig. 2. These replicas increase the azimuth resolution, signal power, and ambiguity. This image is referred to as the observed image.

2.2 Problem awareness

The cell migration range of the target cells was obtained as follows:

$$R(R_0, f_d) = R_0/(1 - (\lambda^2 {f_d}^2/4v^2))^{1/2} \tag{1}$$

where R_0 is the shortest distance between the target and the radar, f_d is the Doppler frequency, λ is the wavelength, and v is the velocity of the platform.

Furthermore, the corrected range of cell migration of the target is discussed, which is obtained as follows:

$$R_t(R_0, f_d) = 0. \tag{2}$$

Furthermore, the corrected range cell migration of the kth azimuth ambiguity is expressed as follows:

$$R_{a,k}(R_0, f_d) = R(R_0, f_d - k f_p) - R(R_0, f_d). \tag{3}$$

Therefore, azimuth ambiguities exist across various range bins, the distributions of the azimuth ambiguities in the Doppler frequency direction differ for each range bin, and the ambiguity components are unevenly distributed.

2.3 Concept

Based on the aforementioned analysis, the concept of the proposed scheme is as follows: The Doppler frequency spectrum S_0 of the observed image s_0 was divided into two parts. These two components were divided at a Doppler frequency of approximately 0 Hz. The obtained spectra S_1 and S_2 were transformed into images, and the obtained images s_1 and s_2 were processed to suppress the azimuth ambiguity. The signal components of the target covered the entire Doppler frequency region of the same range bin. The pixels in which the target exists in each image had large power. However, the azimuth ambiguities were unevenly distributed in each range bin. The power of one pixel was large, whereas that of the other pixel was significantly reduced. Azimuth ambiguities can be reduced by exploiting this property.

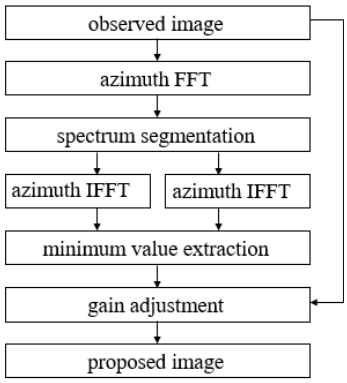

Fig. 3 Process flow of the proposed scheme.

2.4 Processing

This section describes the process flow of the proposed scheme. A block diagram of the specific process flow is shown in Fig. 3. This process comprises azimuth FFT, spectrum segmentation, azimuth inverse (I) FFT, minimum value extraction, and gain adjustment.

The image obtained by inserting 0s in the slow time direction and image processing is denoted by s_0. Suppose $s_i(r,a)$ (i is a natural number) is a pixel at the range bin position r and azimuth bin a in the image s_i. In that case, azimuth FFT is performed on the observed image s_0 to obtain the Doppler spectrum S_0. Thus, the range-Doppler frequency component of the observed image can be obtained.

Spectra S_1 and S_2 were obtained by dividing the spectrum and inserting 0 into the Doppler frequency direction of S_0. In particular, spectrum S_0 is divided in the Doppler frequency direction as follows:

$$S_1(r, f_d) = \begin{cases} S_0(r, f_d) & (-Mf_p/2 \le f_d < 0). \\ 0 & (0 \le f_d < Mf_p/2), \end{cases} \tag{4}$$

$$S_2(r, f_d) = \begin{cases} 0 & (-Mf_p/2 \le f_d < 0). \\ S_0(r, f_d) & (0 \le f_d < Mf_p/2). \end{cases} \tag{5}$$

Azimuth IFFT was performed on each of the two spectra S_1 and S_2 to obtain images s_1 and s_2. The amplitudes of s_1 and s_2 were compared at the pixel position (r,a) and the small value was set as the amplitude of $s_3(r,a)$ to form image s_3 as follows:

$$s_3(r,a) = 2\min(|s_1(r,a)|, |s_2(r,a)|). \tag{6}$$

If azimuth ambiguity is included at pixel position (r,a), either $|s_1(r,a)|$ or $|s_2(r,a)|$ is a small value and $s_3(r,a)$ also is

a small value. Because the azimuth ambiguities are unevenly distributed between images s_1 and s_2, the azimuth ambiguity of s_3 is reduced. The Doppler frequency bands of s_1 and s_2 are half of the total band, therefore the value is also corrected such that it is doubled. The gain g_0 was calculated by comparing s_3 with the absolute value of s_0 as follows:

$$g_0(r,a) = s_3(r,a)/|s_0(r,a)|. \tag{7}$$

If the azimuth ambiguity is included in the pixel position (r,a), $g_0(r,a)$ also decreases because $s_3(r,a)$ is a small value.

Further, g_0 is adjusted by replacing g_1, which has a value greater than 1; with 1, g_1 is generated as follows:

$$g_1(r,a) = \begin{cases} g_0(r,a) & (g_0(r,a) \le 1). \\ 1 & (g_0(r,a) > 1). \end{cases} \tag{8}$$

This operation is aimed at suppressing noise enhancement.

Subsequently, moving average processing of $q \times q$ (q is a natural number) is performed, and the gain obtained is denoted as g_2. To emphasize the azimuth ambiguity suppression effect, g_3 was obtained by calculating the exponentiation with α (α is a real number) as follows:

$$g_3(r,a) = {g_2}^{\alpha}(r,a). \tag{9}$$

g_3 obtained was multiplied by the observed image s_0 to obtain the proposed image s_4.

$$s_4(r,a) = g_3(r,a)s_0(r,a). \tag{10}$$

The pixel containing the azimuth ambiguity indicates a small value in g_3. Therefore, if $s_0(r,a)$ contains azimuth ambiguity, it is multiplied by a small value $g_3(r,a)$ to obtain $s_4(r,a)$. This makes the azimuth ambiguity in the proposed image s_4 less obvious.

Here, we describe the azimuth resolution. The azimuth resolution of the observed image, s_0, increased after the insertion of 0s. The proposed image s_4 is the observed image s_0 multiplied by the gain g_3, which reduces the azimuth ambiguity. Therefore, the proposed image s_4 is not degraded in azimuth resolution relative to the observed image s_0. The proposed image, s_4 maintains a high azimuth resolution after the insertion of 0s.

Moreover, we discuss the S/N ratio. The S/N ratio is increased by the insertion of 0s but does not decrease when processed for the reduction of azimuth ambiguity. The amplitudes of the target from S_1 and S_2 are halved; however, the signal power of the target is not influenced by the doubling in Eq. (6). Conversely, the noise amplitude seems to increase; however, based on simulations, the average amplitude of the noise is not changed by the minimum value selection in Eq. (6) (an additive white Gaussian noise is assumed). Therefore, the S/N ratio is not significantly changed by the azimuth ambiguity suppression process.

Notably, the range resolution of the proposed scheme must be high. This is because the range walking of the azimuth ambiguities in the two split bands does not overlap in the corresponding SAR images. The proposed scheme may not be effective when the range resolution is low.

3. Demonstration

To demonstrate the effectiveness of the proposed scheme, we describe its application to TerraSAR-X data. A reference image of TerraSAR-X with coastal areas, as shown in Fig. 4, was used. This corresponded to an image with $M = 1$, which is the correct image. This image showed Hong Kong, the ocean, the land, and ships on the sea, circled by pink dashed lines. The dynamic range width was ±3 times the standard deviation of the amplitude. This image was decompressed in the azimuth direction, range-cell migration was added, and the data in the slow time direction was thinned with $M = 5$. This simulates the range-compressed raw data at a low PRF. For the data obtained, we inserted 0s, corrected the range cell migration, and compressed the data in the azimuthal direction. The images obtained (observed images) are shown in Fig. 5. The horizontal and vertical axes represent the range and azimuth, respectively. The expected swath of these images was five times that of a conventional SAR image. However, azimuth ambiguity was excessive, and the positions of ships cannot be confirmed. In contrast, the image in Fig. 6 was generated through the proposed scheme for the observed image with $q = 9$ and $\alpha = 10$. The azimuth ambiguities for the land and ships were suppressed in the generated image, and the correct positions of the ships were confirmed.

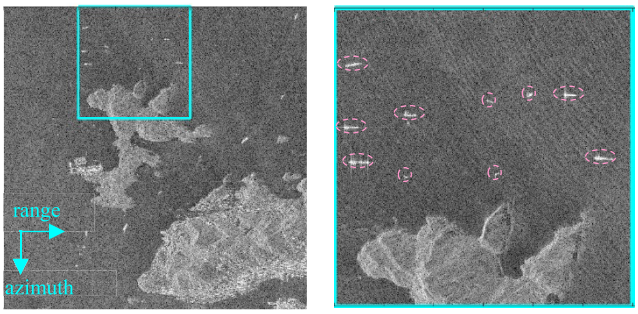

Fig. 4 Reference images ($M = 1$). (left) wide-area image. (right) enlarged image. Pink dashed circles are ships.

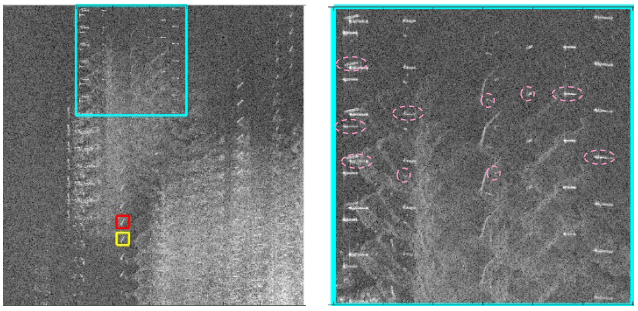

Fig. 5 Observed images ($M = 5$). (left) wide-area image. (right) enlarged image. Pink dashed circles are the truth ships. Red and yellow squares are the regions of ship and the first azimuth ambiguity for calculation of S/A, respectively. Azimuth ambiguities occur along the azimuth.

Here, the effect of suppressing the azimuth ambiguity is validated. Table I summarizes the power of the ship surrounded by the red squares in Fig. 5 (left) and Fig. 6 (left), the power of the yellow square at the first position of azimuth ambiguity generation for this ship, and the signal-to-ambiguity (S/A) power ratio calculated from the results obtained with a changing α. As α increases, the power of target decreases, but azimuth ambiguity decreases more, and the S/A power ratio increases. If α is too large, the azimuth ambiguity decreases very much but extremely reduced signal

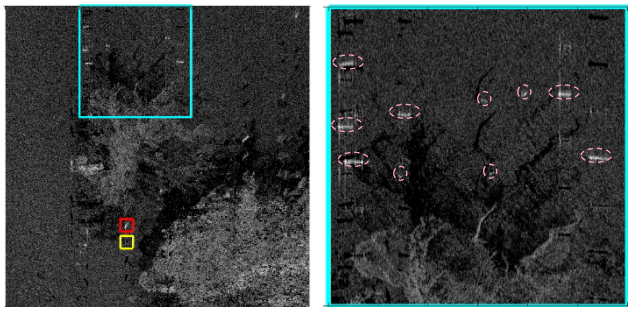

Fig. 6 Proposed images ($M = 5, \alpha = 10$). (left) wide-area image. (right) enlarged image. Pink dashed circles are the ships. Red and yellow squares are the regions of ship and the first azimuth ambiguity for calculation of S/A, respectively. Azimuth ambiguities are reduced.

Table I Evaluation result of the S/A power ratio

	α	Power of the Target [dB]	Power of the ambiguity [dB]	S/A [dB]
Observed	-	64.6	61.9	2.7
Proposed	2	62.8	53.6	9.2
Proposed	5	60.2	43.1	17.1
Proposed	10	55.9	25.5	30.4
Proposed	20	47.3	-3.6	50.9

power increases dark areas. α must be appropriately provided. Therefore, based on the visibility conforming to the dynamic range width, we set $\alpha = 10$ in Fig. 6. Here, it was difficult to set α quantitatively, so it was determined visually. The S/A power ratio was 2.7 dB in the observed image, whereas it increased to 30.4 dB in the proposed image. Thus, the improved gain is 27.7 dB. However, a notable issue is a change in the shape of the island. This is because azimuth ambiguities superimposed on different lands are maintained, as the amplitude of s_3 is not reduced. Furthermore, in Fig. 6 other azimuth ambiguities are also maintained.

4. Conclusion

This study proposed the suppression of azimuth ambiguities for the detection ships on the ocean using satellite-borne SAR. The proposed method suppressed azimuth ambiguity with a high azimuth resolution and S/N ratio by dividing the Doppler frequency spectrum of the observed image into two and processing them. Based on the results obtained using the TerraSAR-X image, the proposed scheme significantly suppressed the azimuth ambiguities through wide-area observation and validated the positions of ships, with an S/A improvement of 27.7 dB. However, azimuth ambiguities superimposed on different targets might be maintained. Reduction in residual azimuth ambiguities and addressing of dark areas are the directions for future research.

References

[1] A. Moreila, P. Prats-Iraola, M. Younis, G. Krieger, I. Hajnsek, and K.P. Papathanassiou, "A tutorial on synthetic aperture radar," *IEEE Geosci. Remote Sens. Mag.*, vol. 1, no. 1, pp. 6–43, March 2013. DOI: 10.1109/MGRS.2013.2248301

[2] I.G. Cumming and F.H. Wong, *Digital Processing of Synthetic Aperture Radar Data: Algorithms and Implementation*, Artech House, Norwood, MA, 2005.

[3] Y. Long, F. Zhao, M. Zheng, G. Jin, H. Zhang, and R. Wang, "A novel azimuth ambiguity suppression method for spaceborne dual-channel SAR-GMTI," *IEEE Geosci. Remote Sens. Lett.*, vol. 18, no. 1, pp. 87–91, Jan. 2021. DOI: 10.1109/LGRS.2020.2967176

[4] D. Velotto, M. Soccorsi, and S. Lehner, "Azimuth ambiguities removal for ship detection using full polarimetric X-band SAR data," Proc. IEEE Int. Geosci Remote Sens. Symp. (IGARSS), pp. 7621–7624, July 2012. DOI: 10.1109/IGARSS.2012.6351863

[5] F. He, Z. Lv, and Z. Sun, "Azimuth ambiguity erasing in spaceborne bistatic SAR images," Proc. 2019 IEEE 4th International Conference on Signal and Image Processing (ICSIP), pp. 841–845, 2019. DOI: 10.1109/SIPROCESS.2019.8868379

[6] A.M. Guarnieri, "Adaptive removal of azimuth ambiguities in SAR images," *IEEE Trans. Geosci. Remote Sens.*, vol. 43, no. 3, pp. 625–633, March 2005. DOI: 10.1109/TGRS.2004.842476

[7] G.D. Martino, A. Iodice, D. Riccio, and G. Ruello, "Filtering of azimuth ambiguity in stripmap synthetic aperture radar images," *IEEE J. Sel. Topics Appl. Earth Observ. Remote Sens.*, vol. 7, no. 9, pp.3967–3978, Sept. 2014. DOI: 10.1109/JSTARS.2014.2320155

[8] Y. Long, F. Zhao, M. Zheng, G. Jin, and H. Zhang, "An azimuth ambiguity suppression method based on local azimuth ambiguity-to-signal ratio estimation," *IEEE Geosci. Remote Sens. Lett.*, vol. 17, no. 12, pp. 2075–2079, Dec. 2020. DOI: 10.1109/LGRS.2019.2963126

[9] G. Krieger, N. Gebert, and A. Moreira, "Unambiguous SAR signal reconstruction from nonuniform displaced phase center sampling," *IEEE Geosci. Remote Sense. Lett.*, vol. 1, no. 4, pp. 260–264, Oct. 2004. DOI: 10.1109/LGRS.2004.832700

[10] R. Horiuchi, T. Hoshino, N. Oishi, and K. Suwa, "Azimuth ambiguity discrimination using Doppler spectrum of the compressive sensing-based SAR image with downsampled PRF," Proc. 2020 17th European Radar Conference (EuRAD), pp. 318–321, Jan. 2021. DOI: 10.1109/EuRAD48048.2021.00088

[11] T. Hoshino, K. Suwa, Y. Yokota, and T. Hara, "Experimental study of compressive sensing for synthetic aperture radar on sub-Nyquist linearly decimated array," Proc. IEEE Int. Geosci Remote Sens. Symp. (IGARSS), pp. 831–834, July 2019. DOI: 10.1109/IGARSS.2019.8900251